

Structural and Optical properties of Mg doped Tungsten oxide prepared by Microwave irradiation method

S. Mohammed Harshulkhan¹  · K. Janaki² · G. Velraj³ · N. Mohanasundaram¹

Received: 27 March 2017 / Accepted: 17 April 2017 / Published online: 28 April 2017
© Springer Science+Business Media New York 2017

Abstract The synthesis of magnesium doped Tungsten oxides (Mg:WO₃) nanomaterial was achieved using a simple household microwave irradiation method. In which 3 and 10 wt% magnesium chloride were used to prepare the above material. The synthesized materials were structurally and optically characterized using various techniques like X-Ray Diffraction, FTIR, UV-DRS, PL and SEM-EDAX. The X-ray diffraction confirms clearly showed the presence of crystalline Mg: WO₃ particles. Further, UV-DRS and FTIR result shows the presence of Mg: WO₃ nanomaterials at specific wavelength. From UV-DRS the optical band gap energy increases to 3–3.15 eV compare to the pure materials. The scanning Electron Microscopy(SEM) analysis confirms that the synthesized Mg:WO₃ was spherical in shape and has 30–40 nm size in diameter. EDAX confirms the Mg doped in the synthesized material. The emission spectra of the undoped and Mg doped samples were analyzed using PL spectroscopy.

1 Introduction

In recent years, the water and air pollutants are removed by photocatalytic technology. Synthesis of transition metal

oxide semiconductor drew a considerable attention due to morphological structure and the exploration of their properties due to their potential application in electronic, optical, super conductor devices, etc. [1]. To decompose pollutants of organic compounds by photocatalytic reaction, the oxidation potential of hole needs to be more positive than +1 V that is redox potential of general organic compounds. In addition, the redox potential of electrons needs to be more negative than that of oxygen (O₂/O₂⁻ or H₂O₂) because surplus electrons that are not consumed by reduction of oxygen would result in electron–hole recombination, which leads to the decreasing photocatalytic activity. The most suitable material for photocatalyst, which also meets these conditions, is TiO₂. The bandgaps of rutile and anatase type TiO₂ is 3.2 eV. The conduction bands are negative enough to reduce oxygen into O²⁻ by one-electron reduction. To decompose the organic compounds are due to the valence band of the semiconducting materials. Photocatalytic reaction was carried out under the UV light irradiation is the serious problem to take into account [2].

Oxide semiconductors with narrow bandgap energy of ≤2.5 eV have a potential for visible-light-driven photocatalyst as well as TiO₂. Generally, the quantum efficiency is lowered due to high probability of electron–hole recombination with narrowing the bandgap. The bandgap energy of WO₃ is 2.5 eV, where the valence band level is almost same as TiO₂, while the conduction band level is much lower than that of TiO₂ and then just able to reduce oxygen to H₂O₂ by two-electron reduction. Since the rate of two-electron reduction of oxygen would be low, resulting in the recombination of electron–hole [3], WO₃ alone was considered to show the low quantum efficiency under visible light irradiation.

A variety of metal oxides like Zinc oxide, Titanium dioxide and tungsten oxide are prepared by different

✉ S. Mohammed Harshulkhan
harshulkhan21@gmail.com

¹ Department of Physics, Vinayaka Mission's Kirupananda Variyar Engineering College, Salem, Tamilnadu 636308, India

² Department of Physics, Government Arts College for Women, Salem, Tamilnadu 636008, India

³ Department of Physics, Anna University, Chennai, Tamilnadu 600025, India

techniques like hydrothermal route [4], surfactant mediated method [5] sol–gel [6], chemical co precipitation [7], acidification method [8], and electrodeposition method [9]. In the above methods, the microwave irradiation method has sparked much interest due to their operation simplicity, effective, low-cost route to synthesis, less time consuming (about 10 min), and for large-scale production [10].

There are several additives and dopants which can improve the photocatalytic performance of WO_3 . Chemical doping of WO_3 with metallic (Cu [11], Sn [12], Pd [13], Mn [14], Ag [15] etc.) elements to modify the electronic structures of semiconductors as well as their surface properties, thus extending their visible light absorbance. In this report, synthesis and systematic investigation of pure and Mg doped WO_3 nanoparticles by microwave irradiation method for the first time. To the best of our knowledge, this is the first preliminary report about structural, optical and photocatalytic activity of pure and Mg doped WO_3 nanoparticles by microwave irradiation method. Moreover, the method is simple, cost effective and less time consuming compared with other methods.

2 Experimental procedure

2.1 Material synthesis

The pure and (3, 10 wt%) of Mg doped tungsten oxide prepared by tungstic acid and magnesium chloride in 10 ml of sodium hydroxide (NaOH) solution. It results in a yellow color solution due to proton exchange process [16]. Then the initial pH value was 10 whereas at the end, the pH was 1. It acts as the medium for the required product to have desired morphology [17]. After attaining the desired pH value, 5 ml of distilled water is added for quick response of microwave with precursor solution. The final solution was placed into the Microwave oven (2.45 GHz) under optimum power of 360 W in air atmosphere. After the irradiation process, the resultant substance was dried in convection mode at 100°C for 5 min. The final product was pale green in color for pure WO_3 and Mg doped WO_3 .

2.2 Characterization techniques

The surface morphology, structural and chemical state of the obtained Nanomaterial was characterized by using X-ray diffraction method (X-ray Diffractometer-XPRT PRO) and FTIR (Spectrum RX I- Perkin Elmer). Optical measurements were carried out in UV–Vis Spectroscopy (SHIMADZU 3600 UV–Vis Spectrometer), Surface morphology was studied by Scanning Electron Microscopy (FEIQUATA250), Elemental analysis were

Table 1 Crystalline size and lattice parameter for pure and Mg doped WO_3

Material	Lattice parameters			Average crystalline size (nm)
	a(Å)	b(Å)	c(Å)	
Pure WO_3	7.3521	7.5351	7.6242	46.35
3 wt% Mg	7.3487	7.5285	7.6191	34.36
10 wt% Mg	7.3401	7.5235	7.6051	32.43

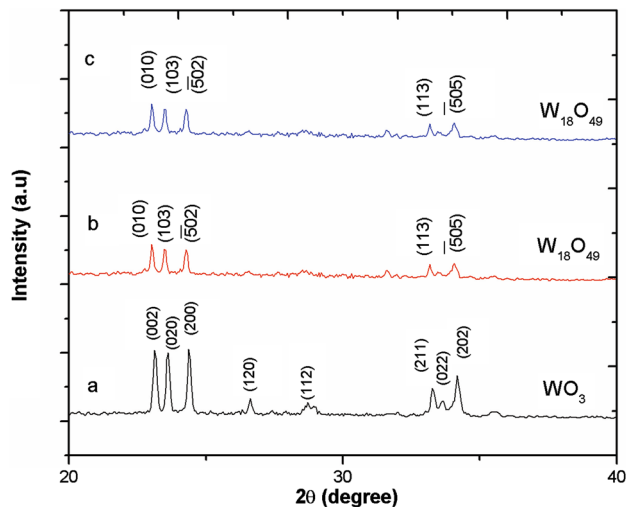


Fig. 1 XRD pattern for **a** Pure WO_3 **b** 3 wt% Mg **c** 10 wt% Mg

performed by EDAX (FEIQUATA250) and PL spectra were recorded by LS 45 Fluorescence spectrometer.

3 Results and discussion

3.1 XRD analysis

The phase formation and purity of the pure and Mg doped WO_3 nanoparticles were investigated by XRD as shown in Fig. 1. From the X-ray analysis, it was noted that the diffraction peaks of the pristine WO_3 at 22.12° , 23.59° , 24.37° , 26.60° , 28.77° , 33.26° , 33.61° and 34.16° could correspond to (002), (020), (200), (120), (112), (022), (202) and (220) planes of WO_3 with monoclinic type crystal structure and the results are in good agreement with the standard JCPDS data (card no: 83-0950). After doping Mg, the diffraction peaks at 23.02° , 23.50° , 24.28° , 33.18° and 34.10° are correspond to (010), (103), (502), (113) and (505) plane of Mg doped tungsten oxide ($\text{W}_{18}\text{O}_{49}$) with monoclinic structure and the result are in good agreement with standard JCPDS data (card no: 84-1516). It was observed that the WO_3 changes to $\text{W}_{18}\text{O}_{49}$ due to the fact that the structure variation between WO_3 and WO_2 leads to change in linking of

coordination polyhedral from corner sharing to edge sharing [18]. Moreover, the intensity of the peak decreases with the increase in the Mg concentrations. These results clearly indicate that Mg^{2+} substituted in WO_3 host lattice site. The lattice parameters of pure WO_3 were estimated at $a=7.3721$ (\AA), $b=7.5451$ (\AA), $c=7.6142$ (\AA) and $b=90.892$. After Mg doping, these parameters decrease with the increase in the Mg concentrations (Table 1), the observed variation in lattice parameters was consistent with the smaller radius of the Mg^{2+} ion (0.734\AA) with respect to the W^{6+} ion radius (0.78\AA) and with the small amount of Mg concentration used for doping.

The average crystalline sizes of the pure and Mg doped WO_3 nanoparticles were calculated by using Scherrer's Eq. [19].

$$D = \frac{0.9\lambda}{\beta \cos\theta} nm$$

where d is the mean crystallite size, K is the shape factor taken as 0.89, k is the wavelength of the incident beam, D is the full width at half maximum and θ is the Bragg angle. The average crystalline size of pristine WO_3 was found to be 46.35 nm and it was further decreased to 34.36 and 32.43 nm for 3 and 10 wt% Mg doped WO_3 . This result suggests that the grain growth is suppressed due to doping of Mg into W-site. Table 1 shows the crystalline size and lattice parameter for pristine and Mg (3 and 10 wt%) doped tungsten oxide materials.

3.2 FTIR analysis

Figure 2 shows the FTIR spectra of pure and Mg doped WO_3 . The recorded wave number and relative intensities obtained from the spectra and the assignments were listed in Table 2. The tungsten oxide vibrations were found in the infrared region of $1453\text{--}600 \text{ cm}^{-1}$ which correspond to W–O stretching, bending and lattice mode. The absorption bands at 3401.74 and 3380.62 cm^{-1} are attributed to stretching vibration of surface hydroxyl group or adsorbed water. It was found due to re-adsorption of water molecules from ambient atmosphere. The peaks around the corresponding wavenumbers 1623.18 , 1629.01 and 1630.45 cm^{-1} are due to W–OH vibration. The spectrum shows strong bands at 828.20 , 837.29

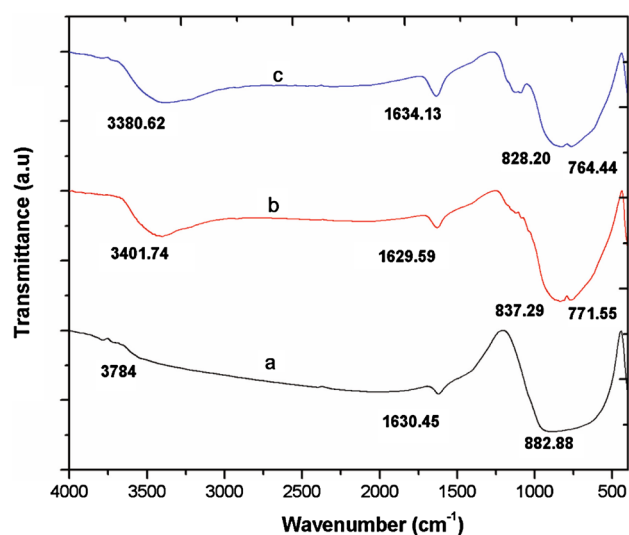


Fig. 2 FTIR spectra for a Pure WO_3 b 3 wt% Mg c 10 wt% Mg

and 882.88 cm^{-1} for W–O–W bridging mode [20]. The 764.44 and 771.65 cm^{-1} band assigned to the out of plane deformation W–O–W mode, when hydrogen was located at a coplanar square of oxygen atoms. After Mg doping these peaks was shifted to lower wavenumbers and this may have been due to the decrease in size of the doped samples.

3.3 UV–Visible diffusion reflectance spectroscopy

Figure 3a–c shows the diffusion reflectance spectra of Pure and Mn doped WO_3 respectively. The absorption from 650 to 450 nm towards lower wavelengths in the entire spectrum (blue shift) corresponds to the absorption edge of the solids. From the Fig. 3b, c it is well observed that the enhancement of bandgap energy is due to the doping of magnesium in the pure WO_3 . This is due to optical transparency of the pure WO_3 increases with the increase in the Mg doped WO_3 . The transmittance of Mg doped WO_3 were increase due to the presence of metal ions (Mg^{2+}). Band gap energy for doped samples were also decreased and bring a considerable blue shift in the absorption edges with the increase of Mg content from 0 to 10 wt%.

Table 2 Observed FTIR spectrum for pure and Co doped WO_3

Reference value	Pure WO_3	3 wt% Mg doped	10 wt% Mg doped	Tentative assignment
3454	–	3401.74	3380.62	O–H stretching mode
1625.98	1630.45	1629.01	1623.18	W–OH vibration
833.21	882.88	837.29	828.20	W–O–W bridging mode
769.29	–	771.65	764.44	W–O–W Stretching and bending mode

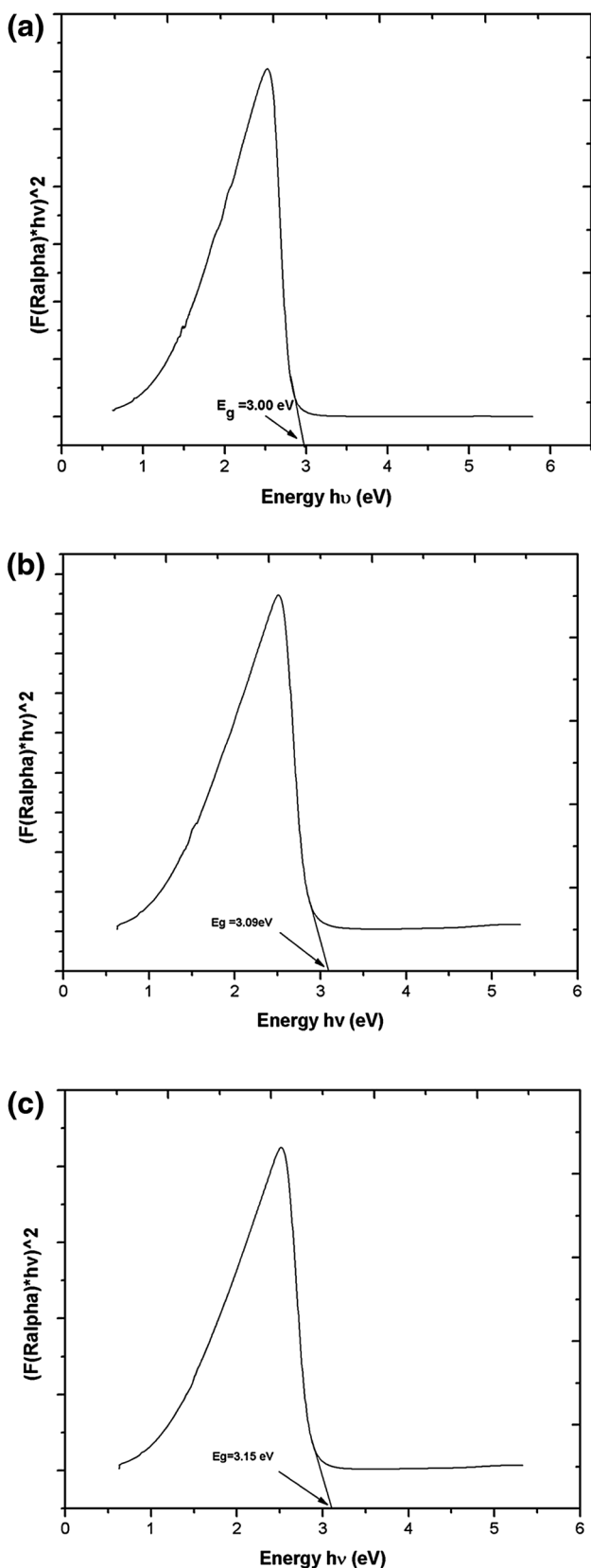


Fig. 3 **a** UV–Visible DRS spectra for Pure WO_3 , **b** UV–Visible DRS spectra for 3 wt% Mg doped WO_3 , **c** UV–Visible DRS spectra for 10 wt% Mg doped WO_3

The band gap energies (E_g) have been calculated using Kubelka–Munk (K–M) model as described below. The K–M model [19] at any wavelength is given by.

$$\frac{K}{S} = \frac{(1 - R_\alpha)^2}{2R_\alpha} = F(R_\alpha)$$

$F(R_\alpha)$ is the so called remission or Kubelka–Munk function, where.

$$\left(R_\alpha = \frac{R_{\text{sample}}}{R_{\text{standard}}} \right)$$

A graph is plotted between $[F(R_\alpha)hv]^2$ vs hv and the intercept value gives the band gap energy E_g [20] of the individual sample. The band gap energies were calculated for pure and 3, 10 wt% Mg doped WO_3 are tabulated. These values offer an excellent agreement with the reported value. The bandgap energy for pure WO_3 is 3.00 eV and further increased for 3 and 10wt% as 3.09 and 3.15 eV.

3.4 Scanning electron microscopy and EDAX analysis

The SEM uses a focused beam of higher energy electrons to generate a variety of signals at the surface of solid specimens. The signals that derive from electron sample interactions reveal information about the sample including external morphology. When sample were viewed under SEM, the spherical morphology with regular size was observed as shown in the Figs. 4b and 5b. The average diameter of 1–1.5 micrometer and thickness of 80–100 nm. After doping of Mg the plate like morphology decreases when increasing the Mg content as shown in the Fig. 5b. The decrease of crystalline size was also confirmed by XRD results. The EDAX results confirm the obtained materials are composed of W and O as shown in the Fig. 4a. Figure 5a shows the EDAX spectra confirms the presence of Mg in the doped material. The intensity peak of tungsten was decreased due to the addition of Mg ions in the tungsten site and intensity peak of oxygen remains constant for both pure and Mg doped WO_3 .

3.5 Photoluminescence studies

The PL spectroscopy is a useful study to measure the energy distribution of emitted photons and to understand the electron hole pair in the semiconducting oxide materials [21]. The oxygen vacancy and lattice distortion of pure and magnesium doped tungsten oxide samples were analyzed using photoluminescence spectra and it is shown in the Fig. 6. The spectra were recorded under the excitation wavelength of 325 nm at room temperature. Both pure and Mg doped tungsten oxide material

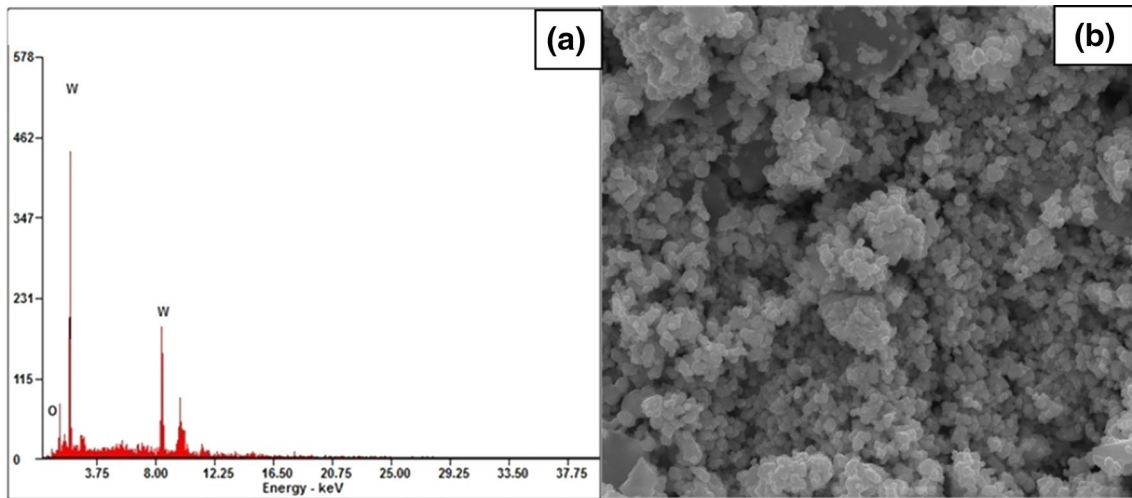


Fig. 4 **a** EDAX image of pure WO_3 , **b** SEM image of pure WO_3

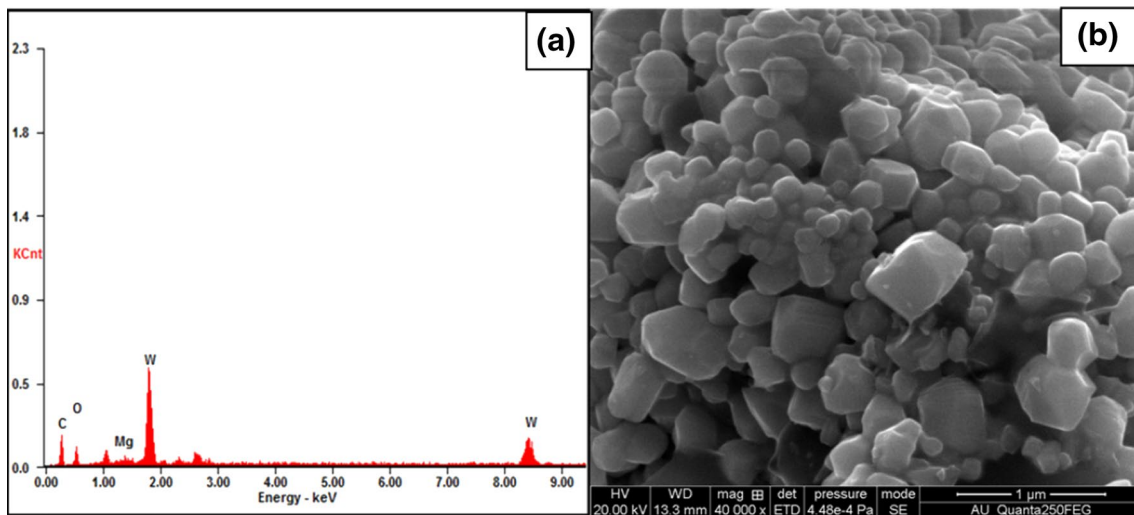


Fig. 5 **a** EDAX spectra of 10 wt% Mg doped WO_3 , **b** SEM image of 10wt% Mg doped WO_3

show blue emission (490–498 nm) and green emission (565–570 nm). The blue emissions are due to the defect level in the bandgap for its electron transition. The green emission peaks is related to v_o^+ oxygen vacancies and these emission may be attributed to the different luminescent centers such as defect energy levels arising due to Mg interstitials and oxygen vacancies as well as dangling bonds into nanocrystals. Due to the Magnesium doped into tungsten oxide, the intensity of peaks decreases and shifted towards the lower energy. The decreases in the peak intensity are due to the presence of Mg into WO_3 and cause the lattice defects.

4 Conclusion

Finally, it has been substantiated that a simple and inexpensive microwave irradiation method is used to synthesize the pure and Mg doped WO_3 . The crystalline size and structure were evaluated from XRD which has monoclinic structure and crystallite which ranges from 32 to 46 nm. The UV-DRS method was used to calculate the bandgap energies of the prepared material and effective with the reported value. UV-DRS analysis shows that the band gap energy increases with the decrease in the particle size. Mg doping into the WO_3 increases the bandgap which is evident by a blue shift

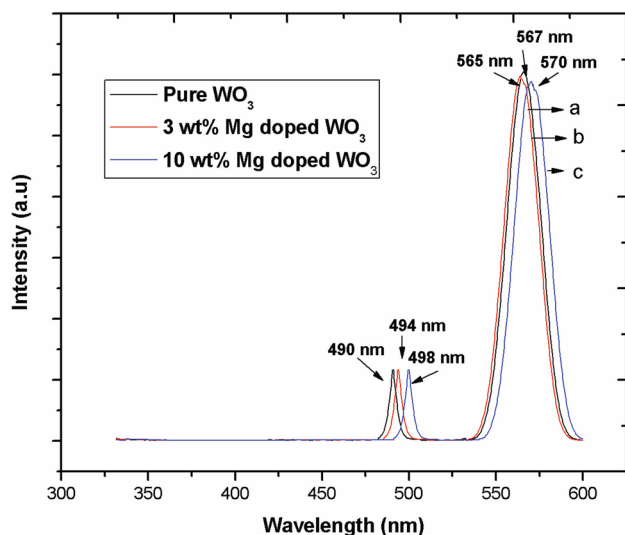


Fig. 6 Photoluminescence spectra for **a** Pure WO_3 **b** 3 wt% Mg **c** 10 wt% Mg

in the optical absorption edge and that was found by UV-DRS method. Scanning Electron microscopy confirms the plate like morphology change as the magnesium concentration increases in the WO_3 . The energy dispersive spectrum confirms the presence of tungsten, oxygen and magnesium in the synthesized materials. The PL studies show the blue shifts in the optical absorption edge and the same was obtained for pure and Mg doped WO_3 . Band gap energy for doped samples were increased and bring a considerable blue shift were observed in the absorption edges with the increase of Mg content into the tungsten site. So, the Mg doped WO_3 can be used in the enhancement of photocatalytic activity in both UV and visible region.

Acknowledgements The author extends his gratefulness to Mr. R. Sakthiganapathy, Mr. S. Krishnaraj, Mr. M. Nagarajan, Mrs. K. Karpagam and Mrs. P. Rajini to provide the moral support. Author also thanks Mr. M. Parthivarman and Mrs. P. Kanchana for their supports rendered during the research work.

References

1. R. Abazari, A.R. Mahjoub, L.A. Saghatforoush, S. Sanati, *Mater. Lett.* **133**, 208–211 (2014)
2. M. Nishikawa, S. Hiura, Y. Mitani, Y. Nosaka, *Trans. GIGAKU*, **1**, 1–6 (2012)
3. R. Abe, K. Sasaki, H. Kunioku, B. Ohtani, *J. Am. Chem. Soc.* **130**, 7780 (2008)
4. J. Ha, P. Muralidharan, D.K. Kim, *J. Alloys Compd.* **475**, 446–451 (2009)
5. N. Asim, S. Radiman, M.A.B. Yarmo Ameri, *J. Appl. Sci.* **6**, 1424–1428 (2009)
6. W. Wang, Y. Pang, S.N.B. Hodgson, *Microporous Mesoporous Mater.* **121**, 121–128 (2009)
7. C. Pang, J. Luo, Z. Guo, T. Huo, *Int. J. Refract. Met. Hard Mater.* **28**, 343–348 (2010)
8. T. Kida, A. Nishiyama, M. Yuasa, K. Shimano, N. Yamazoe, *Sens. Actuators, B* **135**, 568–574 (2009)
9. M. Deepa, M. Kar, D.P. Singh, A.K. Srivastava, S. Ahmad, *Solar Energy Mater. Solar Cells* **92**, 170–178 (2008)
10. M. Parthivarman, K. Vallalperuman, S. Sathishkumar, M. Durairaj, K. Thavamani, *J. Mater. Sci.* **25**, 730–735 (2014)
11. X. Bai, H. Ji, P. Gao, Y. Zhang, X. Sun, *Sens. Actuators, B* **193**, 100–106 (2014)
12. S.B. Upadhyay, R.K. Mishra, P.P. Sahay, *Sens. Actuators, B* **193**, 19–27 (2014)
13. Z. Hua, M. Yuasa, T. Kida, N. Yamazoe, K. Shimano, *Thin Solid Films* **548**, 677–682 (2013)
14. S.M. Harshulkhan, K. Janaki, *J. Mater. Sci.* **26**, 8307–8314 (2015)
15. S.M. Harshulkhan, K. Janaki, G. Velraj, R. Sakthi Ganapathy, M. Nagarajan, *J. Mater. Sci.* **27**, 4744–4751 (2016)
16. A. Wolcott, T.R. Kuykendall, W. chem, S. Chen, J.Z. Zhang, *J. Phys. Chem.* **12110**, 25288–25396 (2006)
17. T. Jesionowski, *Powder Technol.* **127**, 56–65 (2002)
18. V. Von, D. Chemikerin, E. Rodel, A. Berlin, *Genehmigte dissertation. Technical University, Berlin*, pp 16–19 (2006)
19. M.H. SayedAbhudhahir, J. Kandasamy, *Mater. Sci. Semicond. Process.* **40**, 695–700 (2015)
20. I. Hargittai, M. Hargittai, V.P. Spiridonov, E.V. Erokhin, *J. Mol. Struct.* **8**, 31 (1971)
21. P. Wu, Q. Li, X. Zou, W. Cheng, D. Zhang, C. Zhao, C. Lingfei, X. Tan, *J. Phys.* **188**, 8 (2009)